Correlated polarization-switching kinetics in bulk polycrystalline ferroelectrics: A self-consistent mesoscopic switching model

Ruben Khachaturyan,[1,*] Jens Wehner,[2] and Yuri A. Genenko[1,†]

[1]*Institut of Materials Science, Technische Universität Darmstadt, Jovanka-Bontschits-Str. 2, D-64287 Darmstadt, Germany*

[2]*Max Planck Institute for Polymer Research, Ackermannweg 10, 55128 Mainz, Germany*

(Received 28 April 2017; revised manuscript received 28 July 2017; published 17 August 2017)

Analysis of statistical distributions and auto- and cross correlations of polarization and electric field during the field-driven polarization reversal in a bulk polycrystalline ferroelectric is performed. A mesoscopic switching model is used which accounts self-consistently for the development of depolarization fields. Correlations mediated by electrostatic fields are shown to be mostly isotropic and short range at the typical scale of the grain size which is explained by an effective screening via adapting bound charges. The short-range screening clarifies the paradoxical ability of common statistical concepts neglecting the feedback effect of depolarization fields to adequately describe the polarization switching kinetics. The statistical distribution of the local electric field magnitudes is continuously spreading in the course of the global polarization reversal due to mismatching of both dielectric tensor and spontaneous polarization at grain boundaries. The increasing field dispersion substantially contributes to the well-known deceleration of the polarization reversal at long times.

DOI: 10.1103/PhysRevB.96.054113

I. INTRODUCTION

Electric field-driven switching of spontaneous polarization is a fundamental process in ferroelectric materials relevant to many applications, for example digital data storage. Despite the great significance of polarization dynamics for applications, switching mechanisms remain poorly understood even for well-studied ferroelectrics in single crystal or polycrystalline forms. Indeed, the classical picture of polarization switching developed in works by Landauer [1], Miller *et al.* [2], and Ishibashi *et al.* [3] suggests spontaneous nucleation and growth of domains of the opposite polarization within a previously homogeneously polarized medium. Polarization reversal inevitably creates local bound charges due to polarization mismatch at the domain boundaries which, in turn, generate electric depolarization fields. In nonconducting media these large and long-range fields are not expected to be screened. Thus, depolarization fields have to play an essential role in the switching process by providing mutual influence of different switching regions. However, widely used statistical concepts of the polarization switching [3–8] assume independent and uncorrelated nucleation and growth of reversed domains and thus virtually neglect the feedback effect of the depolarization fields during the polarization reversal. Furthermore, the inhomogeneous field mechanism (IFM) model, recently advanced by the authors [9,10] and also assuming independent polarization switching in individual regions, describes the time-dependent response of various ferroelectric ceramics of different chemical compositions and phase symmetries [10–16] as well as of semicrystalline polymers [17] with high accuracy.

Whereas in single-crystalline media the polarization switching may, in principle, occur by moving charge-free 90°-domain walls without generating local bound charges [18,19], avoiding local charges in polycrystalline media, such as bulk ferroelectric ceramics, is impossible because of inevitable mismatches of different crystalline orientation in adjacent grains. A paradoxical ability of statistical concepts, which neglect the feedback of depolarization fields, to accurately describe polarization switching kinetics in a variety of inorganic ferroelectric ceramics [6,7,9–16,20,21], organic ferroelectrics [17,22–27], and organic-inorganic ferroelectric composites [28,29] needs to be comprehended.

Attempts made so far to account for the feedback of depolarization fields remained mostly within the mean-field approximation which assumes emergence of a time-dependent spatially uniform electric field due to averaging of multiple switching events [30–32]. Being an important step towards the understanding of the polarization switching in disordered media such an approach still misses the intrinsically stochastic nature of emerging depolarization fields which are possibly correlated at a finite scale. Particularly, in the case of long-range correlations a spatially and temporally coherent switching could, in principle, keep the depolarization fields small. This would explain, on the one hand, a weak effect of the depolarization field, but mean, on the other hand, that switching in different regions cannot be considered as being independent.

The importance of collective domain dynamics was recognized and studied in thin ferroelectric films for more than a decade by various methods. Strong correlations of domain structures extending across the grain boundaries have been observed by piezoelectric scanning probe microscopy (SPM) in polycrystalline thin films [33] and by transmission electron microscopy (TEM) and piezoresponse force microscopy (PFM) in model single-grain structures [34–36]. Polarization response exhibited clustering ranging from few grains [33] to agglomerations of 10^2–10^3 grains [37,38]. Macroscopic and local measurements of nonlinear behavior in mechanically clamped and released polycrystalline films revealed the dominant role of collective long-range strain interactions mediated by the local and global mechanical boundary conditions, possibly by elastic coupling through the substrate [39,40].

*rubenftf@gmail.com

†genenko@mm.tu-darmstadt.de

Latest *in situ* high-energy x-ray diffraction advances allowed for time resolution of different switching processes in bulk ferroelectric ceramics [41–43]. Furthermore, the grain-resolved three-dimensional x-ray diffraction (3D-XRD) was used to trace the non-180° ferroelectric domain switching within polycrystalline bulk media [44,45]. The collective dynamics in bulk materials was found to be correlated over approximately 10–20 grains, a scale presumably resulting from the complicated and still not understood interplay between the electrostatic field [46] and the elastic strain energy. This moderate characteristic length disagrees with extremely long-range electrostatic correlations predicted for uniform media by phase-field simulations [47] and by a microscopic model describing self-consistently the polarization reversal randomized by thermal vibrations [48]. Thus, the role of long-range electrostatic interactions in the switching dynamics of bulk ferroelectric ceramics still remains unclear.

Recently a self-consistent mesoscopic switching (SMS) model [49] was suggested by the authors which accounts in a self-consistent way for the local depolarization fields. These arise in a random polycrystalline medium leading to the interaction of different regions during the field-driven polarization switching. In the current study, the auto- and cross correlations of random polarization and electric fields and evolution of their statistical distributions are investigated in a polycrystalline ferroelectric by extension of the SMS model. The paper is organized as follows. The model is introduced in Sec. II. Investigation of spatial correlations of electric field and polarization components including their evolution in the course of the total polarization reversal is presented in Sec. III. Associated development of the statistical distribution of the electric field is described in Sec. IV. The results are discussed and concluded in Sec. V.

II. TWO-DIMENSIONAL SELF-CONSISTENT MODEL OF POLARIZATION SWITCHING

An advanced SMS model combines a numerical solution of coarse-grained local equations for polarization development in individual grains with the global calculation of the electric field by the finite-element method (FEM). In the following, the description of a ferroelectric ceramic and the evolution equations are introduced.

A. Creation of a random structure

We consider a polycrystalline bulk ferroelectric placed between two—top and bottom—plain electrodes. The material is assumed to consist of many single-crystalline grains of random shape and position. A representative two-dimensional (2D) structure is created using the Voronoi tessellation around randomly distributed seed points (see an example of the structure in Fig. 1).

Each grain possesses tetragonal phase symmetry and a random crystal orientation uncorrelated with neighbor grains. An initial polarization state is assumed to be created by a very strong electric field applied in positive z direction given by the vertical axis in Fig. 1. In this case, polarization directions in individual grains are arbitrarily chosen from the appropriate three-dimensional angle distribution function for a nonoriented

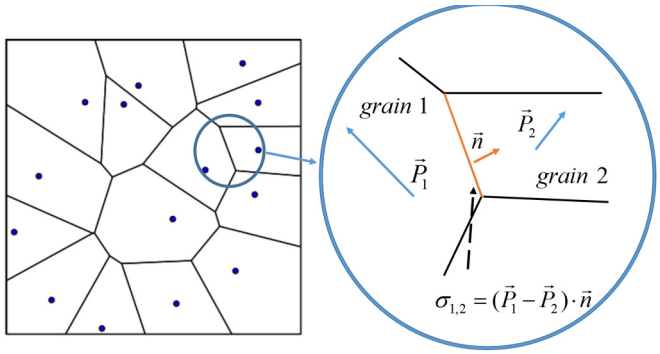

FIG. 1. Voronoi tessellation diagram around 15 randomly located seeds; appearance of a surface bound charge at a grain boundary as a result of mismatching polarizations is shown in the inset.

ferroelectric bulk ceramic of tetragonal symmetry [50]:

$$f(\theta,\varphi) = \begin{cases} \frac{3}{2\pi}, & 0 \leqslant \theta \leqslant \frac{\pi}{4} \\ \frac{6}{\pi^2}\left[\frac{\pi}{4} - \arccos(\cot\theta)\right], & \frac{\pi}{4} < \theta < \theta_{\max} \end{cases} \quad (1)$$

with $\theta_{\max} = \arcsin\sqrt{2/3}$ the threshold angle introduced by Uchida and Ikeda [51]. According to the chosen polarization (c-axis) direction, each grain is characterized by the two-dimensional dielectric tensor $\varepsilon_{ij} = \varepsilon_0 K_{ij}$, with principal values of the relative permittivity K_a and K_c.

Polarization within each grain is substituted by its mean value, $\mathbf{p}_i$, in the hard ferroelectric approximation which entails discontinuities at grain boundaries where surface charge densities arise equal to an abrupt variation of the normal component of the polarization when traversing the boundary (see inset in Fig. 1). The electric field, in contrast, varies within the grains according to the Laplace equation and natural boundary conditions at the grain boundaries which comprise continuity of the tangential electric field and discontinuity of the normal component of the electric displacement equal to the surface charge density. To apply an external electric field of either direction to the system, the top and the bottom lines of the computation box in Fig. 1 are held at constant potentials, whereas periodic boundary conditions are applied to the left and the right side of the box.

B. Evolution equations

The change in the polarization of individual grains is assumed to obey the Kolmogorov-Avrami-Ishibashi (KAI) model of domain nucleation and growth [3–5]:

$$\triangle p(t) = 2P_s\{1 - \exp[-(t/\tau)^\beta]\}, \quad (2)$$

where P_s is the saturation polarization, β is the Avrami index depending on the reversal domain dimensionality, t is the time elapsed after the voltage application, and τ is the switching time. It is well known that τ is strongly dependent on the electric field value E, for example, according to the empiric Merz law $\tau(E) = \tau_0 \exp(E_a/E)$ [52], where E_a is the so-called activation field and τ_0 is the switching time at very high fields.

In the original KAI approach the field E is assumed to be uniform in the whole system and constant in time. In such heterogeneous systems as ferroelectric ceramics the field is of course distributed nonuniformly, at least, due to complying

with the boundary conditions at the grain boundaries. In the spirit of the IFM model [9,10] we suppose that the local switching time $\tau(E)$ is determined by the local value of the electric field E. Over and above, we account for the fact that local switching time values are also time dependent together with the field E. To be able to capture this dependence we substitute the global time dependence of the polarization (2) by the instantaneous rate of the polarization change derived by differentiation of Eq. (2) with respect to the time t:

$$\frac{dp}{dt} = \frac{P_s\,\mathrm{sgn}(E) - p}{\tau}\beta\left(\frac{t}{\tau}\right)^{\beta-1}. \tag{3}$$

Here, the signum function $\mathrm{sgn}(\cdot)$ determines the direction to which the saturation of the polarization proceeds.

Furthermore, the polarization reversal is assumed to be dominated by 180°-switching events, so that the polarization only changes along the chosen c direction within each grain given by a unit vector $\mathbf{n}_i$. This means that the local dielectric tensor remains unchanged during this process. Thus Eq. (3) can be generalized to the vectorial form

$$\frac{d\mathbf{p}_i}{dt} = \frac{\mathbf{n}_i P_s\,\mathrm{sgn}(\langle\mathbf{E}\rangle\cdot\mathbf{n}_i) - \mathbf{p}_i}{\tau(|\langle\mathbf{E}\rangle\cdot\mathbf{n}_i|)}\beta\left[\frac{t}{\tau(|\langle\mathbf{E}\rangle\cdot\mathbf{n}_i|)}\right]^{\beta-1}, \tag{4}$$

where $\langle\mathbf{E}\rangle$ is the value of the electric field averaged over the area of each grain. Equation (4) takes into account that only the field projection on the local c axis promotes switching.

C. Simulation procedure

Simulations include the following steps:

(1) generation of a random geometry (grain forms, c-axes choice)

(2) assignment of material parameters (saturation polarization, activation field, and dielectric permittivity values)

(3) evaluation of the spatial field distribution and average field magnitudes inside each grain using a commercial finite element software FlexPDE from PDE Solutions, Inc.

(4) evaluation of the polarization change during the time step $\triangle t$ by integration of Eq. (4) over $\triangle t$ using the above calculated local average field values and employing the Fehlberg-Cash-Karp method based on the Runge-Kutta approach; consequent updating of polarizations in each grain

(5) calculation of the total polarization by adding up the local modified polarizations weighted by the volume fraction of each grain

(6) transfer of the structure with new polarization values to FlexPDE and repetition of steps 3–5 until the total polarization reaches a saturated value.

A simulation box of the size $20 \times 20\ \mu\mathrm{m}^2$ comprising 400 grains was chosen, which makes up an average linear size of the grain $R \simeq 1\ \mu$m. Material parameters of the tetragonal lead zirconate titanate (PZT) were taken [12] with the activation field $E_a = 35$ kV/mm, $\tau_0 = 5 \times 10^{-11}$ s, and the principal values of the relative dielectric permittivity $K_a = 499$ and $K_c = 198$ as for the tetragonal 40/60 PZT composition [53,54]. The parameter β was set to unity; the choice that does not have a significant effect on the statistical and correlation properties studied below.

Local values of the depolarization field scale with the magnitude of the saturation polarization P_s. When calculated directly from a typical saturation polarization for PZT of $0.45\ \mathrm{C/m}^2$ the field values appear to be unphysically large and therefore should be reduced by various physical mechanisms. A characteristic magnitude of the fluctuation depolarization field ΔE_d due to random charged grain boundaries [50] is as high as $\Delta E_d \simeq 3.5 P_s/4\pi\varepsilon_0\sqrt{K_a K_c} \simeq 50$ kV/mm with the vacuum permittivity ε_0 which is much larger than typical coercive fields for PZT. For low total polarization this high field can be depressed by splitting in domains which leads to low mean polarizations of grains. In a highly polarized state of the ceramic, too high local fields may be depressed due to semiconductor properties of the material. Indeed, the fluctuation field ΔE_d provides a variation of the electrostatic potential across a grain about $\Delta\varphi = \Delta E_d R \simeq 50$ V. Being much larger than the typical band gap in PZT of $E_g \simeq 3.5$ eV such a potential sweep causes strong band bending and produces electron and hole spatial pockets which effectively reduce the mismatch bound charges at grain boundaries. Due to this internal screening effect the local fields cannot exceed a typical value of E_g/qR, with the elementary charge q, so that the potential sweep remains below $E_g/2q$ [55,56]. To account for the internal screening in the calculation of the depolarization fields an effective value of the local saturation polarization $P_s^* = 0.01\ \mathrm{C/m}^2$ is introduced that limits too high charges which may occur at grain boundaries. When delivering the results of solution of Eqs. (4) to the FEM program for evaluation of the spatial field distribution the polarization values are scaled down by a factor of P_s^*/P_s providing the said limitation of the local fields and reasonable switching kinetics.

Polarization reversal was simulated at three applied fields of 3, 4 and 5 kV/mm. The initial state of the system with maximum polarization value P_s in each grain (which results in the total polarization of $0.831 P_s$ [51]) is unphysical since it occasionally includes very unlikely local configurations with highly charged grain boundaries. To start simulations from a physically reasonable initial state the system was first polarized to a saturation value from the initial zero polarization state and then fully re-polarized two times by the change of the voltage

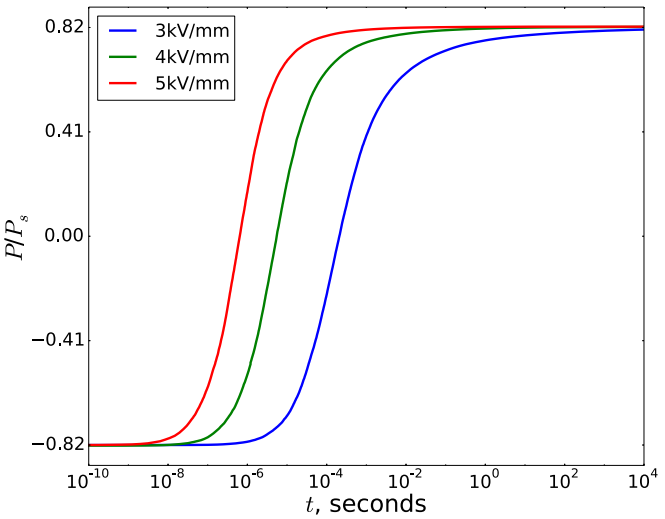

FIG. 2. Time evolution of the total polarization $P = \langle p_z\rangle$ for the Avrami index $\beta = 1$ and different applied voltages as indicated in the plot.

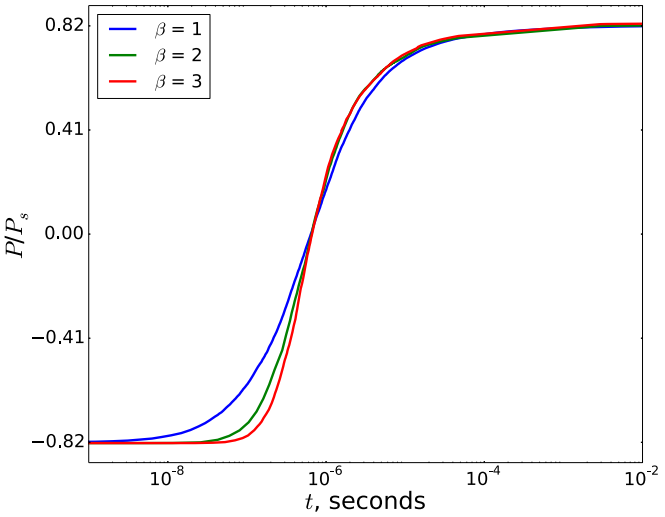

FIG. 3. Time evolution of the total polarization $P = \langle p_z \rangle$ for the applied field of 5 kV/mm and different values of the Avrami index β as indicated in the plot.

sign. These three steps proved to be sufficient to represent a physically valid initial configuration because further full polarization reversals reproduced each other. Time evolution of the total polarization at different applied voltages is presented in Fig. 2.

The choice of the Avrami parameter β has an influence on the kinetics of switching as exemplary calculations for $\beta = 1$, 2, and 3 show in Fig. 3. However, the variation with β vanishes for higher values of β as is expected from the analysis within the IFM model [10] and is confirmed by comparison between curves for $\beta = 2$ and $\beta = 3$ in the latter figure. Since the tests have shown no remarkable changes in statistical and correlation functions for different β, the value $\beta = 1$ was used for simplicity in further simulations.

A polarization map in the saturated state obtained at the applied field of 5 kV/mm is shown in Fig. 4, which reveals that not all grains achieve the saturation state. Local depolarization fields prevent the full polarization reversal thus demonstrating the importance of the local fields for the polarization switching.

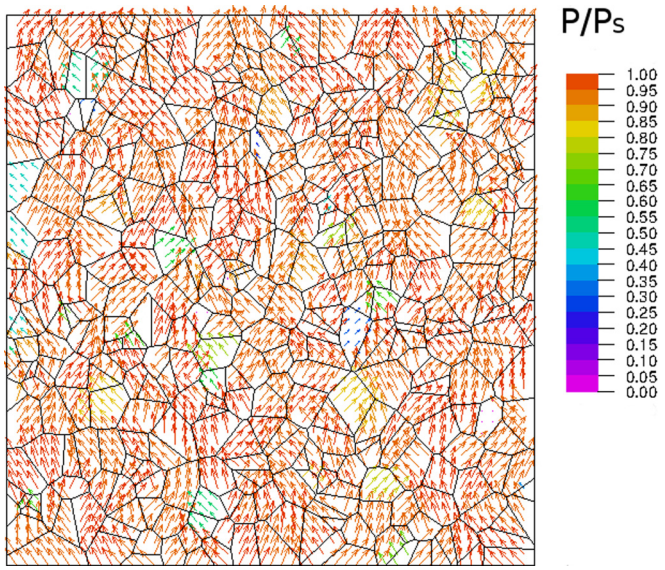

FIG. 4. Polarization map at $P \simeq 0.79 P_s$.

III. CORRELATIONS

To take a closer look into coarse-grained spatial fluctuations of polarization and field we introduce the variance anisotropy factor (VA-factor) as

$$\mathrm{VA(C)} = \frac{\sum_i \sum_j (C_{ij} - \langle C_{\updownarrow j} \rangle)^2}{\sum_i \sum_j (C_{ij} - \langle C_{\leftrightarrow i} \rangle)^2}. \tag{5}$$

Here the values of a spatially dependent variable C_{ij} are evaluated at certain nodes on a quadratic grid of 60×60 points (approximately 9 points per grain) using FlexPDE at different time steps. The values $\langle C_{\updownarrow j} \rangle$ and $\langle C_{\leftrightarrow i} \rangle$ denote the mean values of the variable along the jth column and ith row, respectively. Thus, the VA-factor (5) represents a ratio of mean variances of a physical quantity along and across the applied field direction as is shown in Fig. 5.

In terms of this approach a value of VA close to 1 means that a physical quantity fluctuates similarly in both x- and z-directions, while VA deviation from 1 means that the quantity develops more coherently along (if VA is smaller than 1) or across the field (if VA is larger than 1). The closest analog to the VA factor is the so-called F test in statistics which estimates the ratio of variances of two variables [57]. The absence of correlations of a physical quantity is equivalent to the so-called null hypothesis assuming the VA-factor equal to unity. Disproving the null hypothesis reveals the correlation itself and the correlation anisotropy.

In Fig. 6 the evolution of the VA factor for the variables p_x, p_z, E_x, and E_z is shown during the development of the total polarization value $P = \langle p_z \rangle$ from the maximum negative to the maximum positive value when the field $E_0 = 3$ kV/mm is maintained in the ferroelectric. Here and

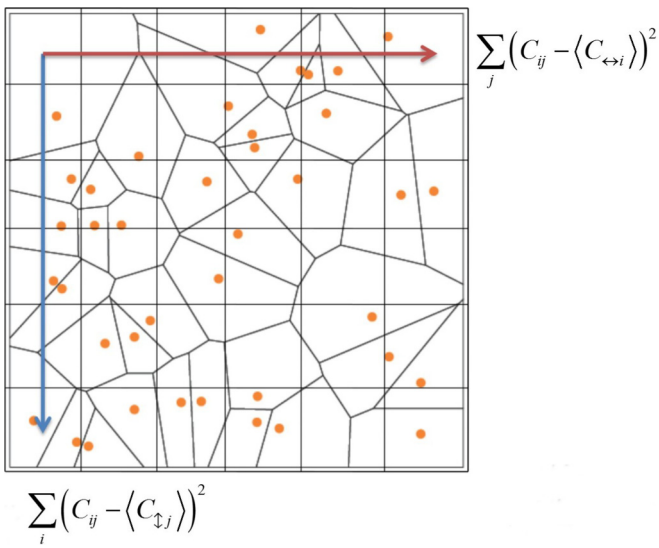

FIG. 5. Scheme of the coarse-grained calculation of the VA factor for a variable C on a quadratic grid. Indexes i and j numerate nodes of the grid.

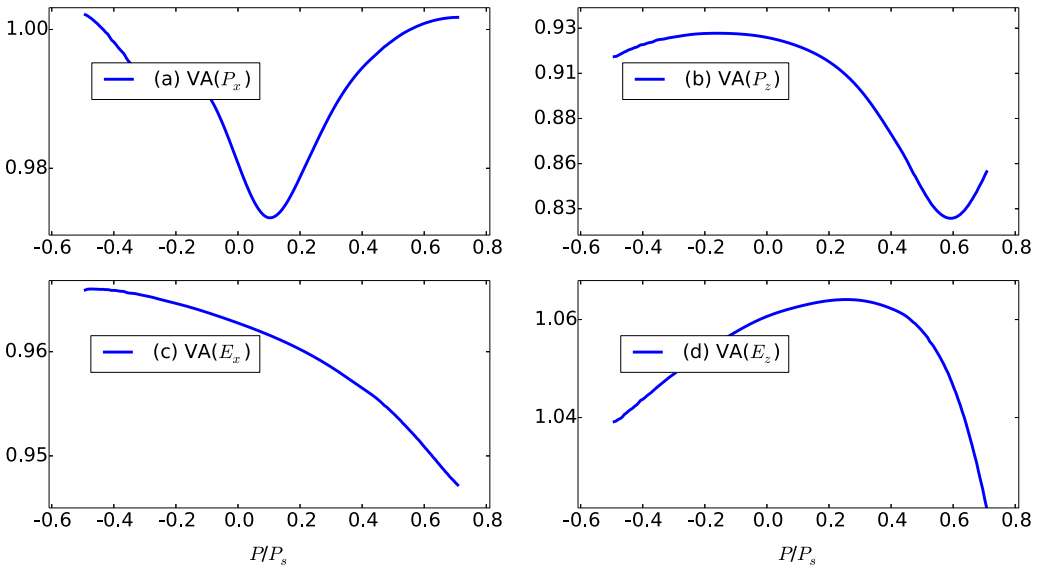

FIG. 6. The VA-factor evolution for (a) p_x, (b) p_z, (c) E_x, (d) E_z components when the total polarization P varies from $-0.7P_s$ to $0.7P_s$.

below the notation of the mean value $\langle ... \rangle$ means averaging over the above introduced 60×60 points grid. It is seen that both components of polarization and electrical field do not obey the null hypothesis exhibiting deviations of the VA factor from unity. The most striking violation of the null hypothesis is observed for p_z component where the VA factor deviates by 20% from unity which is by one order of magnitude larger than for the other variables. This variation of the VA factor is in favor of anisotropic correlations and their evolution during the sample poling. Asymmetric shape of the curves is well reproduced for simulations with different realizations of the random grain structure keeping the same mean grain size. We note that, when poling in the opposite direction the curves in Fig. 6 will be mirrored with respect to $P = 0$.

Based on the results presented in Fig. 6 it is advisable to study spatial autocorrelations of the polarization components, of the electric field components, and cross correlations of the polarization and electric field components at various distances. To this end we use the Pearson two-point correlation

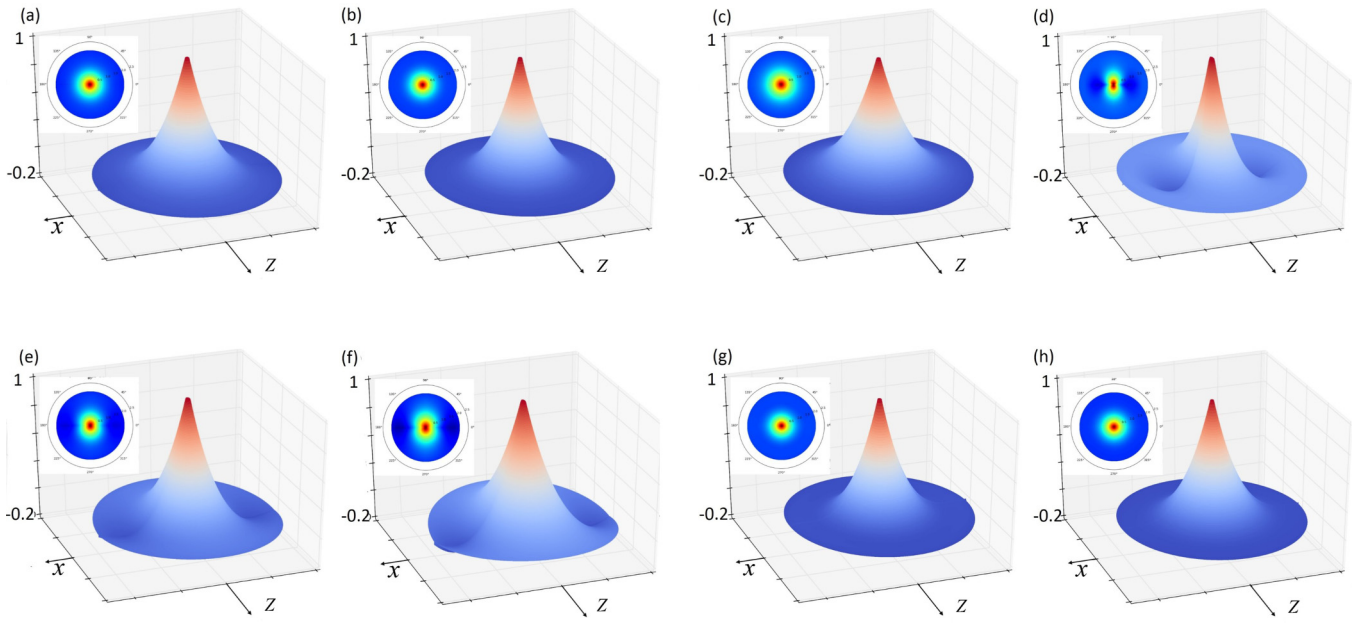

FIG. 7. Correlation coefficients $R(P)$ shown over the area of 2×2 μm^2 at different polarization states $P = \langle p_z \rangle$ when switching from $P = -0.7P_s$ to $0.7P_s$: (a) $R_{p_x,p_x}(0)$, (b) $R_{p_x,p_x}(0.7)$, (c) $R_{p_z,p_z}(0)$, (d) $R_{p_z,p_z}(0.7)$, (e) $R_{E_x,E_x}(0)$, (f) $R_{E_x,E_x}(0.7)$, (g) $R_{E_z,E_z}(0)$, (h) $R_{E_z,E_z}(0.7)$. Electrical field is applied in the negative z direction. The insets in each graph correspond to the view in polar coordinates with colors changing from red to blue when the amplitude of correlation coefficients decreases from 1 to 0.

coefficients defined as

$$R_{E_x,E_x}(\rho) = \frac{\langle E_x(\mathbf{r}+\rho)E_x(\mathbf{r})\rangle}{\langle E_x^2\rangle}, \quad (6)$$

$$R_{E_z,E_z}(\rho) = \frac{\langle E_z(\mathbf{r}+\rho)[E_z(\mathbf{r})-E_0]\rangle}{\langle E_z(\mathbf{r})[E_z(\mathbf{r})-E_0]\rangle}, \quad (7)$$

$$R_{p_x,p_x}(\rho) = \frac{\langle p_x(\mathbf{r}+\rho)p_x(\mathbf{r})\rangle}{\langle p_x^2\rangle}, \quad (8)$$

$$R_{p_z,p_z}(\rho) = \frac{\langle p_z(\mathbf{r}+\rho)[p_z(\mathbf{r})-P]\rangle}{\langle p_z(\mathbf{r})[p_z(\mathbf{r})-P]\rangle}, \quad (9)$$

where the magnitude of the correlation coefficients is bounded by $-1 \leqslant R \leqslant 1$. For strongly correlated quantities $|R| = 1$, while for uncorrelated quantities $R = 0$. The other, non-diagonal autocorrelation coefficients R_{E_x,E_z}, R_{p_x,p_z}, and all cross-correlation coefficients R_{p_α,E_β} appear to be negligible within the calculation error.

Owing to the spatial direction given by the applied electric field the system exhibits macroscopic anisotropy so that a two-point correlation coefficient may depend on the distance vector ρ in the plane (x,z), or on both polar coordinates (ρ,ϕ) in this plane. Correlation coefficients as functions of the distance ρ and angle ϕ are presented in Fig. 7.

The polarization-polarization correlations, as well as field-field correlations, change during the field-driven switching. However, they remain notable only within the range of $\rho \leqslant 1$ μm that corresponds to a neighbor grain distance. An exception is exhibited only by the longitudinal polarization autocorrelations R_{p_z,p_z} which stretch over several μm when $P = -0.6P_s$, see Fig. 8. This polarization stage corresponds to the deepest minimum in the variance anisotropy VA(p_z), as is seen in Fig. 9.

Correlations of the transverse polarization R_{p_x,p_x} [Figs. 7(a) and 7(b)] and of the longitudinal field R_{E_z,E_z} components [Figs. 7(g) and 7(h)] are isotropic in both zero- and high-polarization states. The correlation coefficient for the longitudinal polarization components R_{p_z,p_z} develops from isotropic behavior in the zero-polarization state [Fig. 7(c)] to anisotropic one in the high-polarization state [Fig. 7(d)]. The

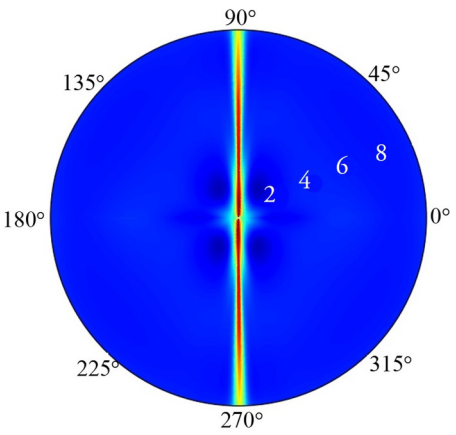

FIG. 8. The correlation coefficient R_{p_z,p_z} in polar coordinates for the total polarization $P = -0.6P_s$ with an electric field applied in the positive z direction. The numbers along the radius ρ indicate distance in μm. The color legend used is the same as in Fig. 7.

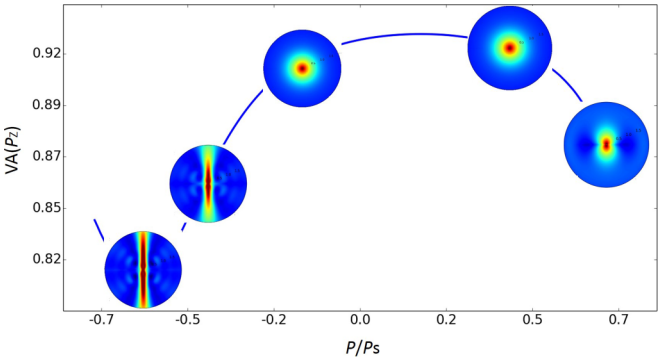

FIG. 9. Evolution of the VA(p_z) factor when the total polarization P varies from $-0.7P_s$ to $0.7P_s$ is shown together with polar plots of the correlation coefficient R_{p_z,p_z} for corresponding polarization stages. The color legend used is the same as in Fig. 7.

correspondence between the VA(p_z) factor and the correlation coefficient R_{p_z,p_z} is displayed in Fig. 9 exhibiting the highest anisotropy in the intermediate stage with $P = -0.6P_s$, as mentioned above. In contrast, correlations of the transverse field components, R_{E_x,E_x}, exhibit remarkable anisotropic features in both zero-polarization and high-polarization state [Figs. 7(e) and 7(f)]. We note here that zero-polarization states result from the field-driven development starting from the high-polarization state and hence retain anisotropic properties. Generally, polarization reversal does not reveal a concerted avalanchelike switching behavior involving hundreds of grains which was sometimes observed in polycrystalline ferroelectric films [37–39]. Consequently this phenomenon cannot be facilitated by electrostatic interactions but is rather provided by long-range elastic interactions as suggested in Refs. [37,40].

IV. ELECTRIC FIELD DISTRIBUTIONS

The spatial distributions of the electric field play an important role in the polarization switching dynamics of polycrystalline systems. Due to the well-known strong field dependence of the switching time [52] different field magnitudes at different locations may provide a substantially retarded or accelerated local switching. Thus, the statistical distributions of switching times may be directly related to the statistical distributions of local electric field magnitudes using the IFM model [9–16]. In this section we analyze the development of the statistical distribution of the local field values $f(E)$ in the course of the polarization reversal.

The electric field is distributed randomly within a polycrystalline ferroelectric for two reasons: random variations in orientation of principal axes of the dielectric tensor in different grains, on the one hand, and random bound charges at grain boundaries due to mismatches of the polarizations in adjacent grains, on the other hand. An example of the spatial field distribution is shown in Fig. 10. Both mentioned factors substantially and independently contribute to the dispersion of the statistical field distribution which is remarkably modified in the course of polarization reversal and the subsequent voltage switching. This can be observed in the following example.

The statistical field distribution for a highly polarized sample was evaluated and compared with the distribution

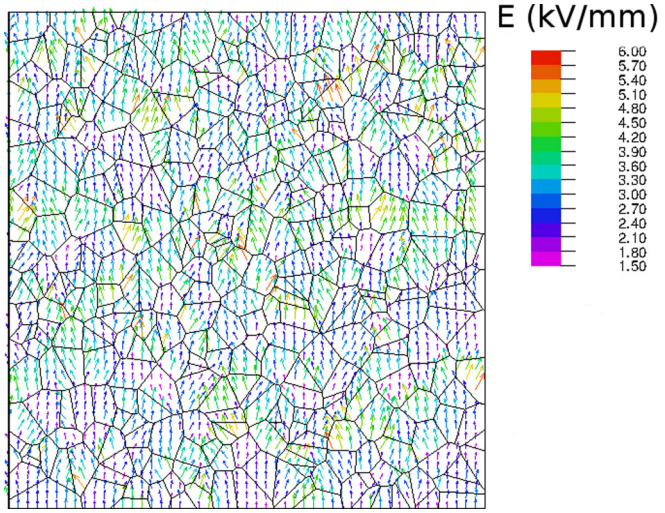

FIG. 10. Field map at an applied field of $E_0 = 3$ kV/mm and the total polarization $P \simeq 0.71P_s$.

immediately after the voltage polarity switching so that the polarization map had not changed yet, see Fig. 11. Though the spatial distributions of both spontaneous polarization and dielectric tensor in a system remain the same the spatial and statistical distributions of the electric field changed remarkably and instantaneously. To comprehend this phenomenon a deeper insight into the nature of the depolarization field is required. For detailed analysis the whole set of field values at all FEM mesh points (10^6) was used.

By the superposition principle, the local electric field at any point of the material can be presented as

$$\mathbf{E} = \mathbf{E}_{\text{ext}} + \Delta_K \mathbf{E} + \langle \mathbf{E}_p \rangle + \Delta_P \mathbf{E}. \tag{10}$$

The first two terms result from the spatial redistribution of the external field applied to the ferroelectric by the charged

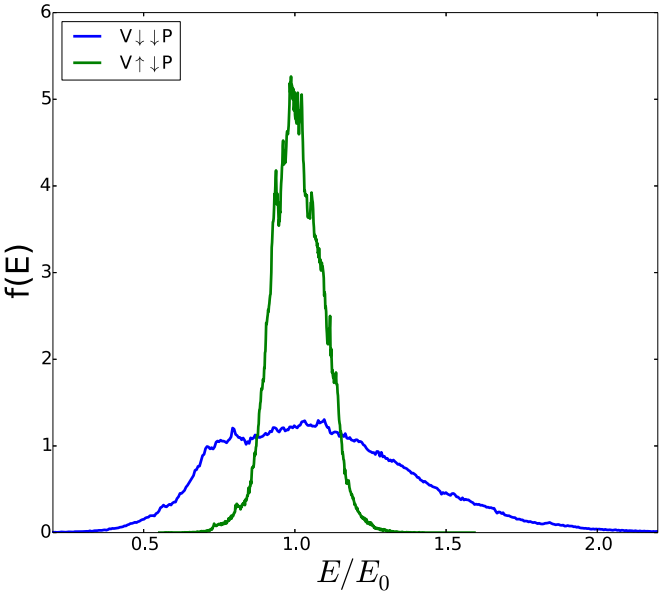

FIG. 11. Statistical field distribution for the saturated highly polarized state before (wider distribution) and after (narrower distribution) the voltage polarity switching.

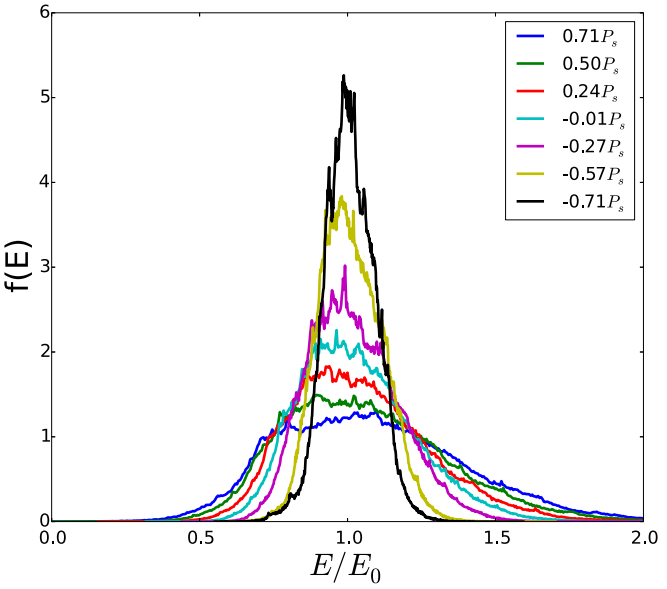

FIG. 12. Evolution of the statistical field distribution with increasing P.

electrodes, whereby $\mathbf{E}_{\text{ext}}$ represents the uniform mean value of the external field in ferroelectric and the spatial fluctuation part obeys the condition $\langle \Delta_K \mathbf{E} \rangle = 0$. Due to linearity of the potential problem the amplitudes of the local spatial field fluctuations $\Delta_K \mathbf{E}$ scale with the magnitude of the external field $\mathbf{E}_{\text{ext}}$. The second two terms in Eq. (10) result from the polarization bound charges and both scale approximately with the total polarization value $P = \langle p_z \rangle$, particularly, the mean value $E_P \simeq -P/\varepsilon_0 \varepsilon_f$ where $\varepsilon_f = \sqrt{K_a K_c}$.

During the polarization reversal the voltage is kept constant together with the mean field in the ferroelectric

$$\frac{V}{L} = E_{\text{ext}} + E_P. \tag{11}$$

Since the total polarization P is changing continuously and eventually changes its sign, the two fields in the right-hand side of Eq. (11) have to change synchronously. This means that with the change of the total polarization from $-P_{\max}$ to $P_{\max}$ the external field E_{ext} should monotonically rise. As the local fluctuation fields $\Delta_K \mathbf{E}$ are scaled together with E_{ext} the field distribution $f(E)$ should increasingly spread due to increasing fluctuation contributions $\Delta_K \mathbf{E}$. Note that at the saturated polarization values both fields E_{ext} and E_P are at their maximum magnitudes so that the dispersion of the field distribution $f(E)$ is a maximum due to both fluctuation fields $\Delta_K \mathbf{E}$ and $\Delta_P \mathbf{E}$. In Fig. 12 such a spreading evolution is observed when the total polarization varies from $-0.71P_s$ to $0.71P_s$.

As soon as the voltage polarity is changed, after reaching the maximum polarization value, Eq. (11) changes to

$$-\frac{V}{L} = E_{\text{ext}} + E_P. \tag{12}$$

Since the value E_P remains unchanged together with the spatial polarization distribution in the system, the external field E_{ext} must be adjusted, thus abruptly reducing its magnitude. This explains the abrupt reduction of the dispersion of the field distribution in Fig. 11. Note that at the end of the polarization

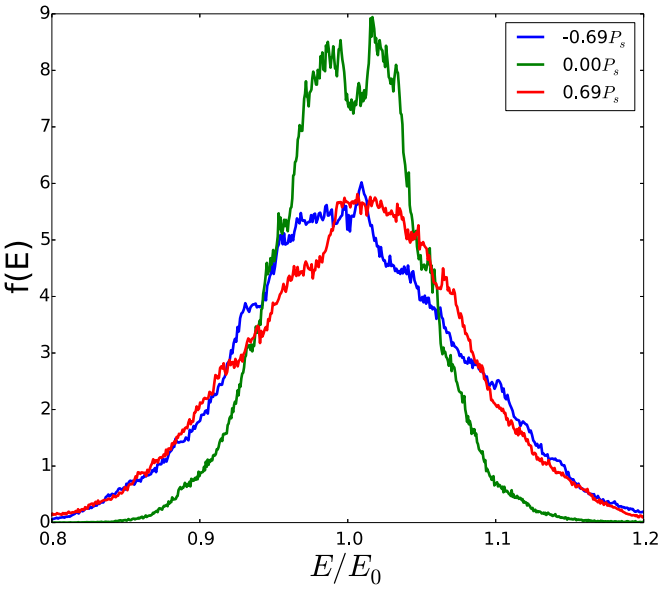

FIG. 13. Statistical field distributions in an isotropic system with $K_a = K_c$.

switching the field E_P is of opposite sign to the external field, while at the onset of the polarization reversal they are of the same sign.

In contrast to the fluctuation field $\Delta_K \mathbf{E}$ the field $\Delta_P \mathbf{E}$ evolves nonmonotonically during the polarization reversal. Since the latter field roughly scales with the total polarization P its dispersion is expected to be at minimum when $P = 0$ and at maximum when polarization reaches its maximum magnitude. Such behavior should be explicitly observed if we neglect the spatial variation of the dielectric tensor. With $\Delta_K \mathbf{E} = 0$ the field fluctuations are caused solely by the polarization variations. Thus the width of the distribution $f(E)$ is minimal when $P = 0$ as is apparent in Fig. 13. The statistical field distributions here roughly exhibit the mirror symmetry with respect to the vertical line $E/E_0 = 1$ indicating the mean field value. This occurs due to local depolarization fields changing their sign together with the total polarization. The symmetry of these distributions is not perfectly bilateral because of the finite size of the random system.

V. DISCUSSION AND CONCLUSIONS

Using the self-consistent mesoscopic switching (SMS) model the correlations of the polarization and the electric field and the statistical distributions of the electric field were studied in the course of the global polarization reversal in a ferroelectric ceramic. Correlation analysis throws some light on the paradoxical ability of statistical concepts neglecting the feedback of depolarization fields to adequately describe polarization switching kinetics.

Two alternative scenarios of depolarization field reduction in disordered polar media are conceivable: highly coherent switching with depolarization fields correlated at a long range, on the one hand, and very short-range correlations of both local polarizations and fields which make switching at different locations effectively independent, on the other hand. The results of the correlation analysis presented in Fig. 7 are clearly in favor of the second scenario. Nevertheless, a question remains as to how the long-range electrostatic interaction is impeded in a nonconducting medium.

The answer seems to hide in the peculiar properties of disordered ferroelectrics. Though these materials are not conducting, local bound charges due to polarization mismatches at grain boundaries are randomly distributed all over the system and possess a considerable mean density. These charges cannot move but are variable. They change in time in order to screen any charge and thus are able to perform the effective Debye screening of the long-range fields. Indeed, a typical surface bound charge resulting from the mean squared fluctuations of the polarization disparity at grain boundaries [50] amounts to $\sigma_P \simeq 0.1 P_s$ which leads to the effective volume density of charge carriers $n_P \simeq \sigma_P/qR \simeq 6 \times 10^{21}$ m^{-3}. Such a high density results in the effective Debye screening length $\lambda_P = \sqrt{\varepsilon_0 \varepsilon_f k_B T/q^2 n_P} \simeq 0.3$ μm comparable to the mean size of grains. This explains the absence of long-range electrostatic field correlations.

Autocorrelations of both polarization and electric field components are mostly isotropic and do not vary essentially during the global polarization switching, while cross correlations of all components remain generally negligible. The only exception from this behavior is given by the autocorrelations of the longitudinal polarization components which occasionally stretch over a dozen grains and undergo remarkable variations in its anisotropy during the polarization reversal. This typical spatial scale of the response appears to be comparable to that observed by 3D-XRD in bulk ferroelectric ceramics [44,45]. Much larger correlation radii are expected for electrostatic reasons in thin ferroelectric films [58]. However, considerably larger clusters of coherent response revealed by PFM and TEM in ferroelectric films [33,37,38] suggest a significant role of the long-range elastic interactions which are not included in the current simulations. We note a substantial difference in correlation behavior between the considered polycrystalline systems and uniform media where long-range electrostatic correlations appear to be dominant as phase-field simulations have demonstrated [47].

Generally, the external electric field remains the original driving force of the global polarization reversal which triggers and dominates the polarization switching at the local and the macroscopic scales. Depolarization fields arising because of mismatches of the local dielectric tensors and spontaneous polarizations in adjacent grains are relevant and not small. They develop in the course of the global polarization switching in a nontrivial way. On the one hand, the dispersion of the statistical distribution of the local electric field values is monotonically increasing during the whole polarization reversal process. On the other hand, the dispersion decreases abruptly after the change of the voltage polarity. An increasing part of locations with substantially reduced electric field magnitudes during the polarization reversal leads to even further retardation of the global switching process with respect to the statistical field distribution alone [9,10] as is already known from the self-consistent quasi-one-dimensional [30] and two-dimensional [49] simulations. However, local switching events may still be considered as independent from each other because of the effective screening of the long-range electrostatic fields.

The obtained results are representative for a wide class of polycrystalline perovskite ferroelectrics. In the presented simulations the material parameters of PZT were used in the calculations. Some of them, such as the saturation polarization and the activation field are not critical for the main conclusions of the paper. In contrast, the anisotropy of the dielectric tensor have a remarkable effect on the statistical field distributions as is seen from the comparison between Fig. 12 (anisotropic case) and Fig. 13 (isotropic case). Anisotropy of the dielectric tensor contributes to the width of the statistical field distributions as discussed in Sec. IV. Thus in more anisotropic materials like $BaTiO_3$ these distributions will be wider. Different realizations of the random grain structure and their initial polarization states do not have a significant effect on the evolution of the VA factor (Fig. 6), correlation functions (Fig. 7–9), and statistical field distributions as long as the mean grain size is kept constant and much smaller than the computation box size, that is important for the quality of the statistical data. The parameter β has a notable effect on the kinetic polarization curves in Fig. 3 making them steeper when higher β is assumed, the effect saturating with increasing β. Different β values have, however, no significant effect on the statistical and correlation functions and the main conclusion on the short-range correlations of the electric field.

Concluding, extremely short spatial correlations of the random electric field and polarization in ferroelectric ceramics explain the apparent absence of the electric interaction between different switching regions. This supports statistical concepts assuming an independent region by region switching in ceramics. This does not mean, however, that the effect of the emerging depolarization fields is negligible. They appear to be comparable in amplitude to the applied field and very much dispersive. This results in the substantial retardation of the global polarization reversal since local polarization switching events are driven by the local fields.

ACKNOWLEDGMENTS

R.K. gratefully acknowledges support from the Deutsche Forschungsgemeinschaft (DFG) through Grant No. GE 1171/7-1.

[1] R. Landauer, J. Appl. Phys. **28**, 227 (1957).
[2] R. C. Miller and G. Weinreich, Phys. Rev. **117**, 1460 (1960).
[3] Y. Ishibashi and Y. Takagi, J. Phys. Soc. Jpn. **31**, 506 (1971).
[4] A. N. Kolmogoroff, Izvestiya Akad. Nauk USSR, Ser. Math. **1**, 355 (1937).
[5] M. Avrami, J. Chem. Phys. **8**, 212 (1940).
[6] A. K. Tagantsev, I. Stolichnov, N. Setter, J. S. Cross, and M. Tsukada, Phys. Rev. B **66**, 214109 (2002).
[7] J. Y. Jo, H. S. Han, J.-G. Yoon, T. K. Song, S.-H. Kim, and T. W. Noh, Phys. Rev. Lett. **99**, 267602 (2007).
[8] D. Kedzierski, E. V. Kirichenko, and V. A. Stephanovich, Phys. Lett. A **375**, 685 (2011).
[9] S. Zhukov, Y. A. Genenko, O. Hirsch, J. Glaum, T. Granzow, and H. von Seggern, Phys. Rev. B **82**, 014109 (2010).
[10] Y. A. Genenko, S. Zhukov, S. V. Yampolskii, J. Schütrumpf, R. Dittmer, W. Jo, H. Kungl, M. J. Hoffmann, and H. von Seggern, Adv. Funct. Mater. **22**, 2058 (2012).
[11] S. Zhukov, Y. A. Genenko, M. Acosta, H. Humburg, W. Jo, J. Rödel, and H. von Seggern, Appl. Phys. Lett. **103**, 152904 (2013).
[12] S. Zhukov, H. Kungl, Y. A. Genenko, and H. von Seggern, J. Appl. Phys. **115**, 014103 (2014).
[13] S. Zhukov, M. Acosta, Y. A. Genenko, and H. von Seggern, J. Appl. Phys. **118**, 134104 (2015).
[14] S. Zhukov, Y. A. Genenko, J. Koruza, J. Schultheiß, H. von Seggern, W. Sakamoto, H. Ichikawa, T. Murata, K. Hayashi, and T. Yogo, Appl. Phys. Lett. **108**, 012907 (2016).
[15] S. Zhukov, J. Glaum, H. Kungl, E. Sapper, R. Dittmer, Y. A. Genenko, and H. von Seggern, J. Appl. Phys. **120**, 064103 (2016).
[16] R. Khachaturyan, S. Zhukov, J. Schultheiß, C. Galassi, C. Reimuth, J. Koruza, H. von Seggern, and Y. A. Genenko, J. Phys. D: Appl. Phys. **50**, 045303 (2017).
[17] J. Schütrumpf, S. Zhukov, Y. A. Genenko, and H. von Seggern, J. Phys. D: Appl. Phys. **45**, 165301 (2012).
[18] B. Jiang, Y. Bai, W. Chu, Y. Su, and L. Qiao, Appl. Phys. Lett. **93**, 152905 (2008).
[19] S. Liu, I. Grinberg, and A. M. Rappe, Nature (London) **534**, 360 (2016).
[20] A. Gruverman, B. J. Rodriguez, C. Dehoff, J. D. Waldrep, A. I. Kingon, and R. J. Nemanich, Appl. Phys. Lett. **87**, 082902 (2005).
[21] J. Y. Jo, S. M. Yang, H. S. Han, D. J. Kim, W. S. Choi, T. W. Noh, T. K. Song, J.-G. Yoon, C.-Y. Koo, J.-H. Cheon, and S.-H. Kim, Appl. Phys. Lett. **92**, 012917 (2008).
[22] A. Nautiyal, K. C. Sekhar, N. P. Pathak, N. Dabra, J. S. Hundal, and R. Nath, Appl. Phys. A **99**, 941 (2010).
[23] N. Dabra, J. S. Hundal, A. Nautiyal, K. C. Sekhar, and R. Nath, J. Appl. Phys. **108**, 024108 (2010).
[24] D. Zhao, I. Katsouras, K. Asadi, P. W. M. Blom, and D. M. de Leeuw, Phys. Rev. B **92**, 214115 (2015).
[25] J. Lee, A. J. J. M. van Breemen, V. Khikhlovskyi, M. Kemerink, R. A. J. Janssen, and G. H. Gelinck, Sci. Rep. **6**, 24407 (2016).
[26] D. Zhao, I. Katsouras, K. Asadi, W. A. Groen, P. W. M. Blom, and D. M. de Leeuw, Appl. Phys. Lett. **108**, 232907 (2016).
[27] A. V. Gorbunov, T. Putzeys, I. Urbanavičiūtė, R. A. J. Janssen, M. Wübbenhorst, R. P. Sijbesma, and M. Kemerink, Phys. Chem. Chem. Phys. **18**, 23663 (2016).
[28] K. C. Sekhar, A. Nautiyal, and R. Nath, Appl. Phys. A **95**, 415 (2009).
[29] N. Mishra, N. Dabra, A. Nautiyal, J. S. Hundal, G. D. Varma, N. P. Pathak, and R. Nath, Ferroelectr. Lett. **42**, 75 (2015).
[30] X. J. Lou, J. Phys.: Condens. Matter **21**, 012207 (2009).
[31] G. Viola, K. B. Chong, F. Guiu, and M. J. Reece, J. Appl. Phys. **115**, 034106 (2014).
[32] K. Auluck and E. C. Kan, IEEE Trans. Electron Devices **63**, 631 (2016).
[33] I. Stolichnov, L. Malin, E. Colla, A. K. Tagantsev, and N. Setter, Appl. Phys. Lett. **86**, 012902 (2005).

[34] D. M. Marincel, H. Zhang, A. Kumar, S. Jesse, S. V. Kalinin, W. M. Rainforth, I. M. Reaney, C. A. Randall, and S. Trolier-McKinstry, Adv. Funct. Mater. **24**, 1409 (2014).
[35] D. M. Marincel, H. R. Zhang, J. Britson, A. Belianinov, S. Jesse, S. V. Kalinin, L. Q. Chen, W. M. Rainforth, I. M. Reaney, C. A. Randall, and S. Trolier-McKinstry, Phys. Rev. B **91**, 134113 (2015).
[36] D. M. Marincel, H. Zhang, S. Jesse, A. Belianinov, M. B. Okatan, S. V. Kalinin, W. M. Rainforth, I. M. Reaney, C. A. Randall, and S. Trolier-McKinstry, J. Am. Ceram. Soc. **98**, 1848 (2015).
[37] P. Bintachitt, S. Trolier-McKinstry, K. Seal, S. Jesse, and S. V. Kalinin, Appl. Phys. Lett. **94**, 042906 (2009).
[38] K. Seal, S. Jesse, M. P. Nikiforov, S. V. Kalinin, I. Fujii, P. Bintachitt, and S. Trolier-McKinstry, Phys. Rev. Lett. **103**, 057601 (2009).
[39] P. Bintachitt, S. Jesse, D. Damjanovic, Y. Han, I. M. Reaney, S. Trolier-McKinstry, and S. V. Kalinin, Proc. Natl. Acad. Sci. USA **107**, 7219 (2010).
[40] F. Griggio, S. Jesse, A. Kumar, O. Ovchinnikov, H. Kim, T. N. Jackson, D. Damjanovic, S. V. Kalinin, and S. Trolier-McKinstry, Phys. Rev. Lett. **108**, 157604 (2012).
[41] J. E. Daniels, C. Cozzan, S. Ukritnukun, G. Tutuncu, J. Andrieux, J. Glaum, C. Dosch, W. Jo, and J. L. Jones, J. Appl. Phys. **115**, 224104 (2014).
[42] S. Gorfman, Crystallogr. Rev. **20**, 210 (2014).
[43] G. Esteves, C. M. Fancher, and J. L. Jones, J. Mater. Res. **30**, 340 (2015).
[44] J. E. Daniels, M. Majkut, Q. Cao, S. Schmidt, J. Wright, W. Jo, and J. Oddershede, Sci. Rep. **6**, 22820 (2016).
[45] M. Majkut, J. E. Daniels, J. P. Wright, S. Schmidt, and J. Oddershede, J. Amer. Ceram. Soc. **100**, 393 (2017).
[46] S. Mantri, J. Oddershede, D. Damjanovic, and J. E. Daniels, Acta Mater. **128**, 400 (2017).
[47] J. E. Zhou, T.-L. Cheng, and Y. U. Wang, J. Appl. Phys. **111**, 024105 (2012).
[48] A. Leschhorn and H. Kliem, J. Appl. Phys. **121**, 014103 (2017).
[49] Y. A. Genenko, J. Wehner, and H. von Seggern, J. Appl. Phys. **114**, 084101 (2013).
[50] Y. A. Genenko, J. Glaum, O. Hirsch, H. Kungl, M. J. Hoffmann, and T. Granzow, Phys. Rev. B **80**, 224109 (2009).
[51] N. Uchida and T. Ikeda, Jpn. J. Appl. Phys., Part 1 **6**, 1079 (1967).
[52] W. J. Merz, Phys. Rev. **95**, 690 (1954).
[53] M. J. Haun, E. Furman, S. J. Jang, and L. E. Cross, Ferroelectrics **99**, 63 (1989).
[54] X. H. Du, U. Belegundu, and K. Uchino, Jpn. J. Appl. Phys., Part 1 **36**, 5580 (1997).
[55] M. Y. Gureev, A. K. Tagantsev, and N. Setter, Phys. Rev. B **83**, 184104 (2011).
[56] Y. A. Genenko, O. Hirsch, and P. Erhart, J. Appl. Phys. **115**, 104102 (2014).
[57] R. G. Lomax and D. L. Hahs-Vaughn, *Statistical Concepts: A Second Course* (Taylor & Francis, New York, 2007).
[58] M. D. Glinchuk, A. N. Morozovska, and E. A. Eliseev, Ferroelectrics **400**, 243 (2010).